In-gas-cell laser ionization spectroscopy of ^{194,196}Os isotopes by using a multireflection time-of-flight mass spectrograph

H. Choi,[1,2,*] Y. Hirayama,[3,†] S. Choi,[1,2] T. Hashimoto,[4] S. C. Jeong,[3,4] H. Miyatake,[3] J. Y. Moon,[4] M. Mukai,[5,6] T. Niwase,[3,6,7] M. Oyaizu,[3] M. Rosenbusch,[3] P. Schury,[3] A. Taniguchi,[8] Y. X. Watanabe,[3] and M. Wada[3]

[1]*Department of Physics and Astronomy, Seoul National University, Seoul 08826, Republic of Korea*
[2]*Institute for Nuclear Particle Astrophysics, Seoul National University, Seoul 08826, Republic of Korea*
[3]*Wako Nuclear Science Center (WNSC), Institute of Particle and Nuclear Studies (IPNS), High Energy Accelerator Research Organization (KEK), Wako, Saitama 351-0198, Japan*
[4]*Rare Isotope Science Project, Institute for Basic Science (IBS), Daejeon 305-811, Republic of Korea*
[5]*Graduate School of Pure and Applied Sciences, University of Tsukuba, Tsukuba, Ibaraki 305-0006, Japan*
[6]*Nishina Center for Accelerator-Based Science, RIKEN, Wako, Saitama 351-0198, Japan*
[7]*Department of Physics, Kyushu University, Nishi-ku, Fukuoka 819-0395, Japan*
[8]*Institute for Integrated Radiation and Nuclear Science, Kyoto University, Kumatori, Osaka 590-0494, Japan*

(Received 1 June 2020; accepted 17 August 2020; published 8 September 2020)

We performed in-gas-cell laser ionization spectroscopy of ^{194,196}Os, which were produced by multinucleon transfer reactions at the KEK Isotope Separation System (KISS). The nuclei of interest were identified through β-decay spectroscopy and a newly applied multireflection time-of-flight mass spectrograph (MRTOF-MS). From the study of laser resonance spectra, isotope shifts (ISs) of the transition $\lambda_1 = 247.758$ nm for ^{194}Os and ^{196}Os were measured for the first time. The change in the mean-square charge radius $\delta\langle r^2\rangle^{192,A}$ and the quadrupole deformation parameter $\langle\beta_2^2\rangle^{1/2}$ were deduced from the IS measurements. The results were compared with the theoretical calculations and the predicted shape transition at ^{194}Os is discussed.

DOI: 10.1103/PhysRevC.102.034309

I. INTRODUCTION

There is a long-standing interest in neutron-rich Os-Pt nuclei in the region of $A \approx 190$, where a shape transition has been predicted. The lighter isotopes in this region are prolately deformed in their ground states and become oblate as the spherical shell closure at $N = 126$ is approached [1–3]. In Pt ($Z = 78$) isotopes, the shape transition takes place quite gradually through the triaxial γ-soft isotopes $A = 184$–196 to oblate neutron-rich isotopes $A = 198$–202 [4]. In the case of Os ($Z = 76$), it is expected to occur suddenly at $A = 192$–194 [5–7]. However, the exact point where the change occurs in the Os isotopic chain has not yet been determined. Wheldon *et al.* [8] suggested that the shape transition occurs at ^{194}Os, in contrast to the earlier interpretation of Casten *et al.* [9]. On the other hand, the possibility of prolate-to-oblate transition at ^{192}Os has been discussed by other theoretical studies [6,7,10]. Nomura *et al.* [7,10] predicted the shape evolution from the prolate deformed ^{190}Os to the oblate ^{194}Os, passing through the γ-soft nucleus of ^{192}Os, from interacting boson model (IBM) calculations.

To resolve the theoretical disagreements, we have applied the powerful method of laser spectroscopy to investigate the nuclear structure in this region. By measuring changes in the atomic transition energy, known as isotope shift (IS), the change in mean-square charge radius, $\delta\langle r^2\rangle$, and the quadrupole deformation parameter, $\langle\beta_2^2\rangle^{1/2}$, can be extracted. Moreover, the measurement of hyperfine structure gives direct access to nuclear properties such as spin and magnetic dipole and electric quadrupole moments. Therefore, such measurements on transitional nuclei help us to understand how nuclear shape changes when approaching $N = 126$. To date, several laser spectroscopy studies of Os nuclei have been done [11–14], but little experimental information is known for neutron-rich isotopes due to the difficulty in their production.

In this paper, we report the first measurement of isotope shift for ^{194,196}Os through in-gas-cell laser spectroscopy [15–19]. These nuclei were produced by multinucleon transfer reactions and extracted using the KEK Isotope Separation System (KISS) [20–22]. The implantation rates of laser-ionized ^{194,196}Os were measured as a function of laser wavelength and their laser resonance spectra were studied to evaluate isotope shifts. The measurements were performed via two methods: β-decay spectroscopy and time-of-flight mass spectrometry. The β-decay spectroscopy was performed with a multisegmented proportional gas counter (MSPGC) [23], while time-of-flight mass spectrometry utilized a multireflection time-of-flight mass spectrograph (MRTOF-MS) [24]. The MRTOF-MS is a powerful device to perform laser spectroscopy on long-lived isotopes ($T_{1/2} > 30$ min) as the measurement duration is independent of the half-lives and the online beam time is not consumed by extended periods of decay measurements [25–27]. From the evaluated isotope shift, we deduced corresponding isotopic variation in

*hyunsuki92@snu.ac.kr
†yoshikazu.hirayama@kek.jp

the mean-square charge radius $\delta\langle r^2\rangle^{192,A}$ and the quadrupole deformation parameter $\langle\beta_2^2\rangle^{1/2}$ based on the pairing-plus-quadrupole model [28]. Finally, we discuss the nuclear structure from the comparison between the present results and theoretical predictions.

II. EXPERIMENT

A. Apparatus

The experiment was performed with KISS [20–22], which is an argon-gas-cell-based laser ion source combined with an online isotope separator, installed at RIKEN Nishina Center. The $^{136}Xe^{20+}$ primary beam (10.75 MeV/A, 50 particle-nA), accelerated by the RIKEN Ring Cyclotron, impinged on a rotating ^{198}Pt target (enriched to 91.63%) with a thickness of 12.5 mg/cm^2. The unstable nuclei ^{194,196}Os were produced by multinucleon transfer (MNT) reactions [29]. The reaction products were implanted, thermalized, and neutralized in a doughnut-shaped argon-filled gas cell [22] with a pressure of 67 kPa.

The neutralized isotopes were re-ionized in the gas cell by a two-color two-step resonant laser ionization technique, allowing nuclei with the specific atomic number Z to be selected. A frequency-tunable dye laser (Radiant Dyes Laser; NarrowScan) pumped by a XeCl:excimer laser ($\lambda = 307.9$ nm, Lambda Physik LPX240i) was used for the first step excitation ($\lambda_1 = 247.758$ nm) with a laser power of 100 μJ/pulse. The wavelength of the dye laser was monitored by a wavemeter WS6 (HighFinesse), which is precisely calibrated with another wavemeter WS7 (HighFinesse). A second excimer laser of the same model, operated with a laser power of 12 mJ/pulse and a pulse duration time of 15 ns, was used for the ionization transition to the continuum. The intense ionization laser causes unwanted line-shape distortions and line broadening in a resonance spectrum [30]. To avoid such effects, the timing of the ionization laser was delayed about 10 ns from the excitation laser. Then, the laser ionized atoms were extracted as singly charged ions, $^{194,196}Os^+$, from the gas cell. The ions were accelerated to an energy of 20 keV, and the mass-to-charge ratio (A/q) was selected by a dipole magnet with mass resolving power of $R_m = 900$. Finally, the isotope of interest was transported to the detector station located in the adjacent experimental hall.

The detector station is divided into two parts. One is the long-standing β-γ detection system and the other is the newly installed MRTOF-MS [24]. During the experiment, the low energy beam extracted from the KISS gas cell (hereafter, KISS beam) can be delivered to either side by use of an electric deflector. The ions transported to the β-γ station were implanted on a 12 μm thick aluminized Mylar tape surrounded by the high-efficiency and low background β-ray detector, MSPGC [23]. The tape was moved at the beginning of each measurement cycle (every 15 min in the present measurements for ^{196}Os) to avoid unwanted radioactivity from the detection area. The gas counter is sensitive to not only β rays but also characteristic x rays and internal conversion electrons, which can be identified by analyzing the multiplicity (M) of the gas-counter hit patterns [23]. In this experiment, the gas counter was used as a β telescope ($M = 2$) whose absolute detection efficiency is as high as about 30% for β rays emitted from ^{196}Os. Four super clover Ge detectors (Canberra, fourfold 32 segmented superclover HPGe) were installed to detect β-delayed γ rays. The absolute detection efficiency was calibrated using ^{152}Eu and ^{133}Ba γ sources and the efficiency was measured to be about 14% for 400-keV γ rays.

So far, heavy nuclei have been identified via decay spectroscopy by measuring specific decay properties, such as γ rays and half-lives. However, it becomes untenable to use decay measurements if the particle's half-life is excessive, such as in the case of ^{194}Os ($T_{1/2} = 6.0$ yr). To overcome this, we used the MRTOF-MS to identify ^{194,196}Os efficiently in real time, without the need to wait for decays, and thereby quickly measured the laser resonance spectra of each. MRTOF-MSs have been widely used as an isobar separator [31–33] and for precise mass measurements thanks to its mass resolving power $R_m > 100\,000$ and the fast measurement time (within 30 ms for each cycle) [34–38]. These capabilities make MRTOF-MS a powerful tool not only for mass measurements but also for identifying heavy nuclei in laser spectroscopy.

The KISS beam, delivered to the MRTOF-MS station, was injected into the 2 mm diameter entrance orifice of the gas-cell-based ion cooler-buncher (GCCB). The GCCB is at room temperature and filled with 100 Pa helium gas. The injected ions were thermalized by collision with helium atoms and extracted by a radio frequency (RF) carpet [24]. Since the second ionization potential (IP) of the Os atom is well below the first IP of He, the collisional interactions strip additional charges from Os^+, resulting in about 80% of ions being extracted in the doubly charged state. The extraction yield of the doubly charged ions was estimated by using a ^{198}Pt KISS beam [39]. The extracted ions were transported by a segmented quadrupole ion guide to a triplet ion trap suite, consisting of a pair of linear Paul traps on either side of a flat trap. In the trap system, ions were accumulated, cooled, and bunched. Then, the ion bunches were orthogonally ejected from the central flat trap and entered the MRTOF-MS. The ions were allowed to reflect back and forth in the MRTOF-MS for a predetermined time, leading to $n = 385$ oscillations in the present measurements, before being released to an ion detector (MagneToF). Due to the multireflection nature of the MRTOF-MS, two ion species with different mass-to-charge ratios can have the same TOF by chance when the difference in mass-to-charge ratio is sufficient to result in different numbers of oscillations [40]. To avoid such misidentifications, confirmation measurements with different number of laps ($n = 384$) were done for each analyte ion. To calibrate the MRTOF-MS, the trap system provides reference ions, typically $^{133}Cs^+$ or $^{85,87}Rb^+$, from a thermal ion source. The measurement of reference ions were interleaved with that of analyte ions with a total cycle of 30 ms. Ions of each were continuously accumulated in their respective Paul traps and alternately transferred to the central trap, in a method we call concomitant referencing [35].

B. Method

In the experiment, the implantation rates of laser-ionized ^{194,196}Os atoms were measured as a function of excitation

laser wavelength and the resonance spectra were studied to evaluate isotope shifts. To identify the laser ionized Os isotopes, two separate methods were used. One is the conventional β-decay measurement method and the other is the newly applied time-of-flight mass measurement by the MRTOF-MS. The fast measurement cycle of the MRTOF-MS allowed us to identify long-lived isotopes, such as ^{194}Os ($T_{1/2} = 6.0$ yr), in a limited online experiment period.

For the decay measurement, the mass-to-charge ratio of the dipole magnet was adjusted to transport $A/q = 196$ ions and the lasers were tuned to ionize ^{196}Os ($T_{1/2} = 34.9$ min). Then, the ^{196}Os ions from KISS were accumulated during 15 min for each laser wavelength. The growth curves of β rays, which originate from ^{196}Os and other contaminant ions, were measured by MSPGC with the hit pattern of $M = 2$. From the fitting analysis of β-ray growth curves, the pure implantation rate of ^{196}Os was deduced.

^{194}Os and ^{196}Os were identified from their mass measurement by using the MRTOF-MS. Based on the internal calibrant ^{85}Rb^{+}, the MRTOF-MS was tuned for ^{194,196}Os^{2+} to achieve maximum mass resolving power of $R_m \approx 120\,000$ at $n = 385$ laps. Then, the TOF data of ions with a mass-to-charge ratios of $A/q = 97$ and 98 were accumulated for 5 mins for each excitation laser wavelength. In the TOF spectra, ^{194,196}Os^{2+} were found with the known mass and TOF of the reference ion, and conditions for fitting analysis were made. From the fit of MRTOF spectra, the number of Os ions was deduced. Finally, the laser resonance spectra of ^{194,196}Os, obtained by two independent methods, were analyzed with a simultaneous fitting procedure and the isotope shifts were evaluated.

III. DATA ANALYSIS

A. Laser resonance spectrum deduced from β-ray growth curve analysis

Figure 1 shows a typical β-decay growth curve for ^{196}Os. The detected β rays originated from the decay of ^{196}Os, its daughter nuclei ^{196}Ir, and some contaminants, mainly ^{196}Ir, which has a constant implantation rate without regard to the excitation laser. Considering the implantation of ^{196}Os and the contaminant ^{196}Ir, the decay process can be described by the following equations:

$$\frac{dN_{\mathrm{Os}}(t)}{dt} = I_{\mathrm{Os}} - \lambda_{\mathrm{Os}} N_{\mathrm{Os}}, \tag{1}$$

$$\frac{dN_{\mathrm{Ir}}(t)}{dt} = I_{\mathrm{Ir}} - \lambda_{\mathrm{Ir}} N_{\mathrm{Ir}} + \lambda_{\mathrm{Os}} N_{\mathrm{Os}}, \tag{2}$$

where $N_i(t)$, λ_i, and I_i ($i =$ Os or Ir) are the number of ions of a given nucleus as a function of the measurement time t, its decay constant, and implantation rate, respectively. The decay rates of β rays from ^{196}Os and ^{196}Ir detected by MSPGC are given as the product of detection efficiency $\epsilon_{\beta,i}$, decay constant λ_i, and $N_i(t)$ ($i =$ Os or Ir):

$$f(t) = \epsilon_{\beta,\mathrm{Os}} \lambda_{\mathrm{Os}} N_{\mathrm{Os}}(t), \tag{3}$$

$$g(t) = \epsilon_{\beta,\mathrm{Ir}} \lambda_{\mathrm{Ir}} N_{\mathrm{Ir}}(t). \tag{4}$$

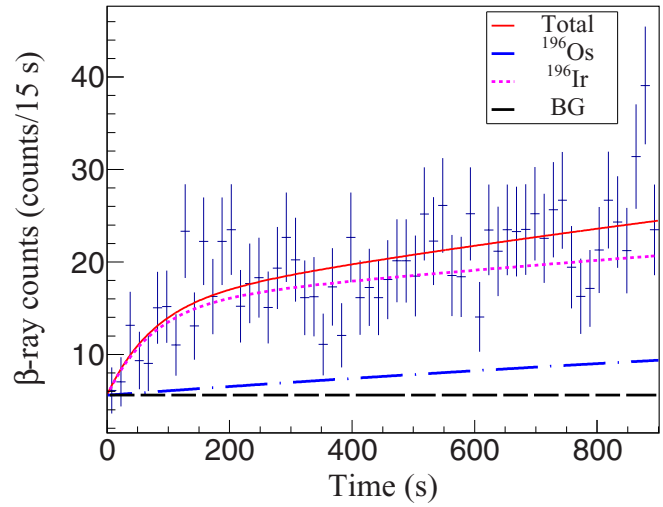

FIG. 1. Typical β-ray growth curve of ^{196}Os nuclei, which was measured using the MSPGC ($M = 2$). The red solid line indicates the total fitting function, which consists of the β-decay growth of ^{196}Os (dash-dotted blue), ^{196}Ir (dotted pink line), and the constant background (long-dashed black line).

Here, the detection efficiencies $\epsilon_{\beta,i}$ were evaluated using GEANT4 simulation [23]. The β-decay growth curve was fitted with the combined function of $f(t)$, $g(t)$, and the constant background I_{BG}, as shown in Fig. 1. In the fitting analysis, I_{Os}, I_{Ir}, and I_{BG} were always free parameters, and the decay constants of ^{196}Os and ^{196}Ir were fixed as $\lambda_i = \ln(2)/T_{1/2}$ from their half-lives of $T_{1/2} = 34.9$ min [41] and $T_{1/2} = 52$ s [42], respectively. The average value of reduced χ^2 for each measurement was around 1.29 in the range of 0.9–2.03. Finally the resonance spectrum of ^{196}Os was obtained as shown in Fig. 2(a) and we confirmed that the contaminant ^{196}Ir is insensitive to the excitation laser, as shown in Fig. 2(b). The implantation rate of contaminant ^{196}Ir is fitted to be 1.57(13) particles-per-second (pps) with the reduced-χ^2 value of 1.0.

B. Laser resonance spectrum deduced from analysis of MRTOF spectra

Figures 3(a) and 3(b) show typical MRTOF spectra of the ions with mass-to-charge ratios of $A/q = 97$ and 98, respectively. In the spectra, isobaric ions, such as Os, Ir, Pt, and Au, were identified by MRTOF-MS. Among them, only the Os ion was produced by resonant in-gas-cell laser ionization. The others, having a constant production rate without regard to the laser irradiation, were likely produced by radiation fields in the region immediately following the KISS gas cell. Figure 3(c) shows a TOF spectrum of the reference ion, ^{85}Rb^{+}, which is used as an internal calibrant.

The fit function for the ion peaks was determined from the TOF spectrum of the reference ion. The ion peaks have non-Gaussian shapes with tails towards larger flight times, as shown in Fig. 3(c), due to the higher-order optical aberrations in the mirrors and low-angle scattering from the residual gas [43]. To describe the asymmetric shape, a Gaussian hybrid function with two exponential tails was used, as described

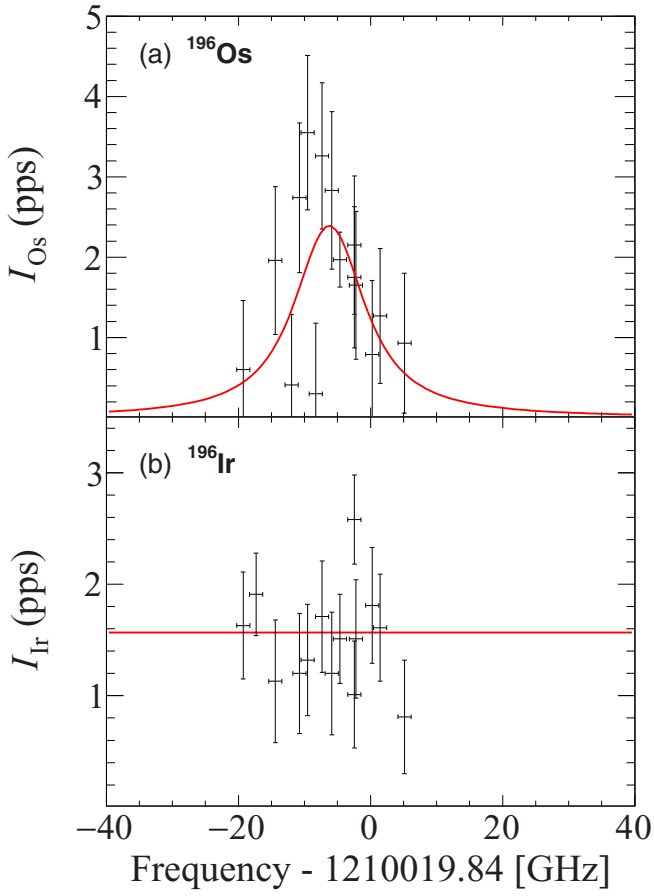

FIG. 2. (a) and (b) are the resonance spectra of the ^{196}Os and ^{196}Ir, respectively. The horizontal axis indicates the laser detuning relative to the transition frequency $\nu_0 = 1210019.84$ GHz ($\lambda_1 = 247.7583$ nm). The red line in (a) is the best-fit result of simultaneous fitting analysis of the ^{194,196}Os resonance spectra. The implantation rate of ^{196}Ir is independent of the laser frequency, and, therefore, the rate is fitted as a constant indicated by the red line.

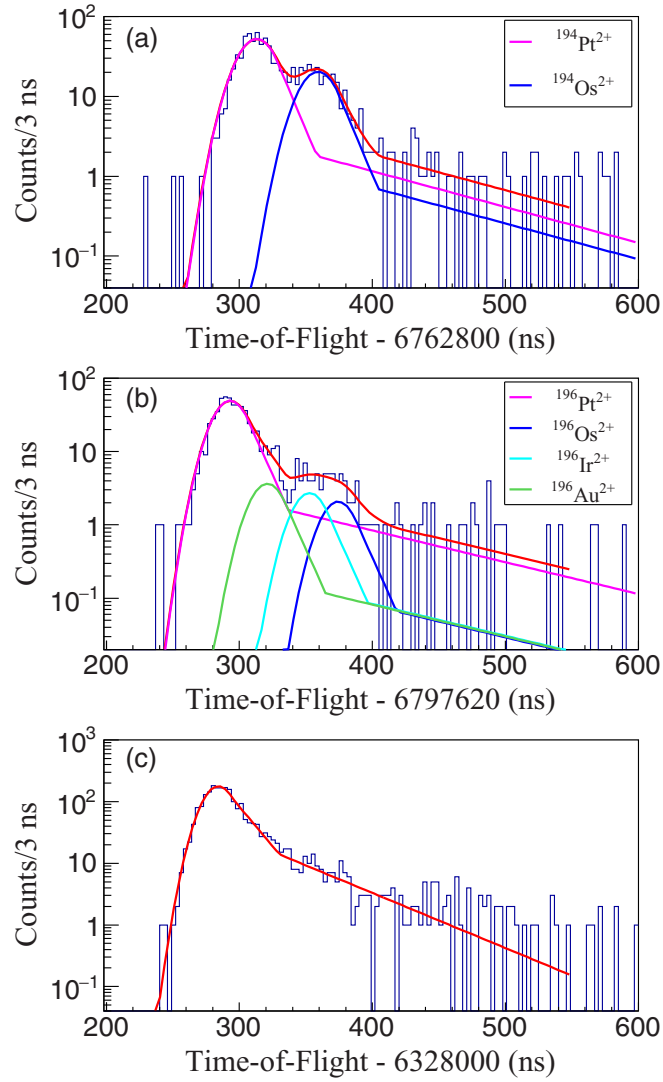

FIG. 3. Typical time-of-flight spectra of the ions with the mass-to-charge ratios of (a) $A/q = 97$, (b) $A/q = 98$, and (c) the reference ion $^{85}Rb^{+}$ after $n = 385$ laps in the MRTOF. The shape parameters for the fitting function were determined with the Pt^{2+} peak (pink line) in the TOF spectrum.

in Eq. (5). The first exponential tail starts at the switching point of $t_1 = t_m + \sigma$, and the extended second tail appears at $t_2 = t_m + \sigma + t_c$, where t_c is the TOF interval between t_1 and t_2:

$$h(t) = A \times \begin{cases} e^{(-(t-t_m)^2/2\sigma^2)} & \text{for } t \leqslant t_1 \\ e^{(-\frac{1}{\tau_1}(t-t_1)-\frac{1}{2})} & \text{for } t_1 \leqslant t \leqslant t_2, \\ e^{(-\frac{1}{\tau_2}(t-t_2)-\frac{1}{2}-\frac{t_c}{\tau_1})} & \text{for } t \geqslant t_2. \end{cases} \quad (5)$$

Here, A is the amplitude, t_m is the position of the maximum of the fit function, σ is the standard deviation of the Gaussian, and τ_i (1 or 2) is the slope of the first or second exponential tail.

The time of flight t of the ion with mass m and charge q was calculated using

$$m = \frac{q}{q_{\text{ref}}} m_{\text{ref}} \left(\frac{t - t_0}{t_{\text{ref}} - t_0} \right)^2, \quad (6)$$

where m_{ref} and q_{ref} are the mass and the charge of the reference ion, respectively. The constant time offset t_0 is the delay between the TDC start signal and the actual ejection of the ions from the MRTOF-MS ion trap. The offset time is determined from the measured TOF and the known masses [44] of Pt^{2+} and $^{85}Rb^{+}$. It is evaluated to be 188(10) ns.

As the isobaric neighbors of $^{194}Pt^{2+}$ are closely packed, the spectra of $A/q = 97$ ions, shown in Fig. 3(a), exhibits only two distinct peaks. The first peak [$t = 6\,763\,112(1)$ ns at $n = 385$ laps] is produced by $^{194}Pt^{2+}$, while the second peak [$t = 6\,763\,160(1)$ ns at $n = 385$ laps] is an admixture of $^{194}Os^{2+}$, $^{194}Ir^{2+}$, and $^{194}Au^{2+}$. The peak centers of these three ions, as calculated by Eq. (6), vary by $\approx$5 ns, and therefore cannot be independently fitted but must be treated as a single spectral peak in the fitting process. Hence, the sum of two hybrid Gaussian functions with the same shape (having the same σ, τ, and t_c) was used for fitting. In the analysis, all the free parameters σ, τ, t_m, t_c were determined from the fit of $^{194}Pt^{2+}$ peak, and these were applied to the other spectral

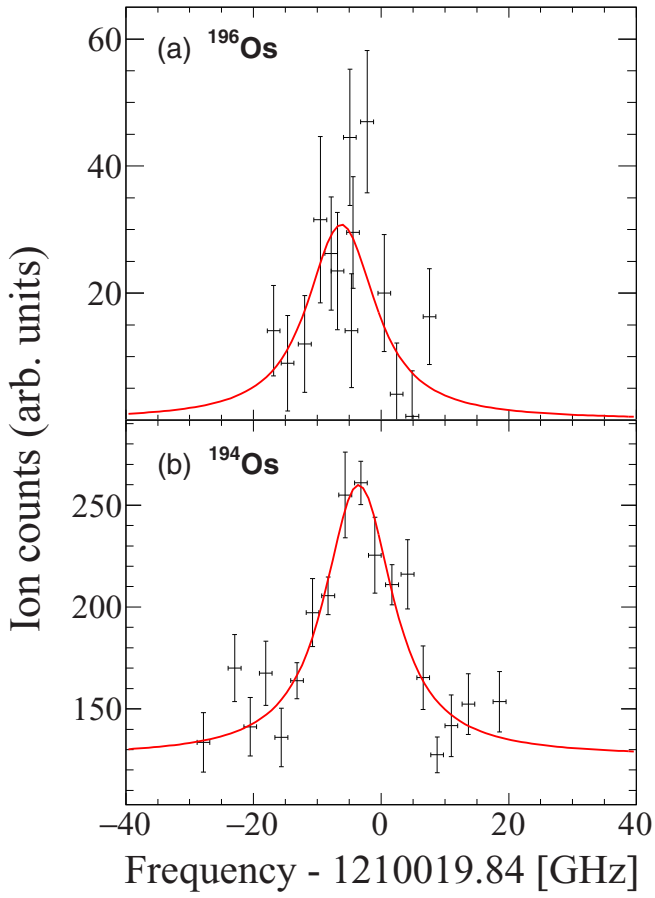

FIG. 4. (a) and (b) are the resonance spectra of ^{196}Os and ^{194}Os, respectively, obtained by evaluating the Os^{2+} ion counts from the TOF specta of MRTOF-MS. The horizontal axis indicates the laser detuning relative to the transition frequency $\nu_0 = 12\,10019.84$ GHz ($\lambda_1 = 247.7583$ nm). The red lines are the best-fit result of the simultaneous fitting analysis.

peak. As the rate of $^{194}Ir^{2+}$ and $^{194}Au^{2+}$ would be independent of laser frequency, the resonance spectrum for $^{194}Os^{2+}$, shown in Fig. 4(b), was determined from the total count rate of the spectral peak at $t = 6\,763\,160(1)$ ns. The large background is the result of the unresolved Ir and Au ions. The error bars are derived from the error matrix calculated by the ROOT MINUIT library [45].

In the case of $A/q = 98$, the calculated TOF intervals between ions were over 20 ns. Therefore the sum of four hybrid Gaussian functions with the same shape was used for fitting. The analysis was done in the same way as explained above in the case of $A/q = 97$. Finally we could obtain the resonance spectrum for ^{194}Os and ^{196}Os as shown in Figs. 4(a) and 4(b), respectively.

C. Resonance spectra analysis

Figures 2(a) and 4 show the resonance spectra of ^{194}Os and ^{196}Os obtained from the β-decay growth curve and MRTOF-MS TOF spectra, respectively. Since there is no hyperfine splitting for even-A Os with $I^\pi = 0^+$, single resonance peaks were observed. The line shape for the resonance peaks can be expressed as a Voigt function, which is a convolution of Gaussian and Lorentzian components. The Gaussian width consists of Doppler broadening and laser linewidth, whose full-width at half maximum (FWHM) values were evaluated to be 1.0 GHz at 300 K and 3.4 GHz, respectively [14]. As a result, a total Gaussian width of 3.5 GHz was used as a fixed parameter in all fitting analysis. The Lorentzian components consisted of a gas-pressure broadening, laser power broadening, and the 2.6 MHz natural width of the present transition. The Lorentzian width Γ_L was a free parameter in this analysis.

The resonance spectra were simultaneously fitted by Voigt functions with common free parameters of Lorentzian width Γ_L for Figs. 2(a), 4(a), and 4(b) and peak position (corresponding to isotope shift value) for Figs. 2(a) and 4(a). The fitting analysis was performed using the ROOT MINUIT library [45]. The reduced-χ^2 of the simultaneous fitting result was 1.25. From the fitting, Γ_L was deduced to be 11.8 ± 1.8 GHz. As a result, a total FWHM of 12.8 ± 3.4 GHz was obtained, which is consistent with the previous study [14]. The values of resonance peak position for ^{194}Os and ^{194}Os were determined to be $\nu^{194} = -3.53(58)$ GHz and $\nu^{196} = -6.24(95)$ GHz at the gas cell pressure of 67 kPa with the offset frequency of 1 210 019.84 GHz. To evaluate the isotope shift, the previously measured value [14] of $\nu^{192} = -0.33(22)$ GHz at the pressure of 17 kPa was used for the reference. Considering the gas pressure shift of $-51(4)$ MHz/kPa [14], the resonance peak positions are evaluated to be $\nu^{194} = -0.98(61)$ GHz and $\nu^{196} = -3.69(97)$ GHz at the pressure of 17 kPa. Finally, the isotope shifts for ^{194}Os and ^{196}Os from the reference isotope ^{192}Os are deduced to be $\nu^{194} - \nu^{192} = -0.65(65)$ GHz and $\nu^{196} - \nu^{192} = -3.36(99)$ GHz, respectively.

IV. RESULTS AND DISCUSSION

From the isotope shift of ^{194,196}Os, corresponding isotopic variation in the mean-square charge radius $\delta\langle r^2\rangle^{192,A}$ and the quadrupole deformation parameter $\langle\beta_2^2\rangle^{1/2}$ were evaluated. Then, the nuclear structure of ^{194,196}Os could be discussed from the comparison between the obtained results and theoretical predictions.

A. Isotope shift

The IS between two isotopes A, A' in a transition i is the sum of the mass shift (MS) and the field shift (FS):

$$\delta\nu_i^{A,A'} = \delta\nu_{\rm MS} + \delta\nu_{\rm FS}.$$

The MS is composed of the normal mass shift (NMS) and the specific mass shift (SMS):

$$\delta\nu_{\rm MS} = (K_{\rm NMS} + K_{\rm SMS}) \times \frac{A' - A}{AA'}.$$

In the $s^2 \rightarrow sp$ transition the contribution of SMS is supposed to be as small as (0 ± 0.5) NMS [46]. Neglecting the SMS, the MS is simply rewritten as

$$\delta\nu_{\rm MS} = \frac{1}{1836.1}\nu_i \times \frac{m_{A'} - m_A}{m_A m_{A'}}$$

where $\nu_i = 1\,210\,019.84$ GHz is a transition frequency. The FS is expressed as the product of electronic factor F_i and the

nuclear parameter λ:

$$\delta\nu_{\rm FS} = F_i\lambda.$$

The value of F for the transition $\lambda_1 = 247.7583$ nm is evaluated by Hirayama [14] as $F_{247} = 20.5 \pm 1.76$ GHz fm^{-2} and is used for the following analysis. The nuclear parameter λ is the sum of the change in the mean-square charge radius and its higher-order terms:

$$\lambda = \delta\langle r^2\rangle + \frac{C_2}{C_1}\delta\langle r^4\rangle + \frac{C_3}{C_1}\delta\langle r^6\rangle + \cdots, \quad (7)$$

where C_i are the electronic coefficients calculated by Seltzer [47] for the K x-ray transitions. Here, the Seltzer values of C_i

$$\frac{C_2}{C_1} = -1.02\times10^{-3}\,\text{fm}^{-2}, \quad \frac{C_3}{C_1} = +2.74\times10^{-6}\,\text{fm}^{-4}$$

are used. The change in the mean-square charge radius is considered as the result of the change in the spherical volume and the shape [48]:

$$\delta\langle r^2\rangle = \delta\langle r^2\rangle_{\rm sph} + \delta\langle r^2\rangle_{\rm def}. \quad (8)$$

The deformation term $\delta\langle r^2\rangle_{\rm def}$ includes dynamic deformations and higher-order multipole contributions. Employing the "pairing-plus-quadrupole model" [28], where the nuclei are described as a uniformly charged axially deformed rotor, the higher-order contribution can be omitted and be reduced to the quadrupole deformation, resulting in [49]

$$\delta\langle r^2\rangle = \delta\langle r^2\rangle_{\rm sph} + \frac{5}{4\pi}\langle r^2\rangle_{\rm sph}\delta\langle\beta_2^2\rangle. \quad (9)$$

Considering the higher-order terms of Eq. (7) up to $\langle r^6\rangle$, the nuclear parameter λ can be rewritten as [49]

$$\lambda = (1+x)\delta\langle r^2\rangle_{\rm sph} + (1+y)\frac{5}{4\pi}\langle r^2\rangle_{\rm sph}\delta\langle\beta_2^2\rangle \quad (10)$$

with

$$x = \frac{C_2}{C_1}\frac{10}{7}R^2 + \frac{C_3}{C_1}\frac{5}{3}R^4,$$
$$y = \frac{C_2}{C_1}2R^2 + \frac{C_3}{C_1}3R^4,$$

where $R = 1.2\bar{A}^{1/3}$ fm, $\bar{A} = (A + A')/2$, is the average radius of the nucleus. Using Seltzer values of C_i, we obtain $x = -0.059$ and $y = -0.079$ for Os ($A = 192$). The spherical mean-square charge radius $\langle r^2\rangle_{\rm sph}$ and its variation $\delta\langle r^2\rangle_{\rm sph}$ were calculated using the droplet model [50]. The quadrupole deformation parameter $\langle\beta_2^2\rangle^{1/2}$ was evaluated with the known value of $\beta_2 = 0.1667(12)$ [51] of the reference isotope ^{192}Os, as described in Eq. (11):

$$\langle\beta_2^2\rangle^{1/2} = \sqrt{\delta\langle\beta_2^2\rangle + \beta_2^2(A=192)}. \quad (11)$$

Finally, $\delta\langle r^2\rangle^{192,194} = 0.034(35)$ fm^2 and $\delta\langle r^2\rangle^{192,196} = 0.177(55)$ fm^2 were obtained from $\delta\nu^{192,194} = -0.65(65)$ GHz and $\delta\nu^{192,196} = -3.36(99)$ GHz, respectively. The $\langle\beta_2^2\rangle^{1/2}$ for ^{194}Os and ^{196}Os were evaluated to be 0.147(10) and 0.157(15), respectively. The results are shown in Table I.

TABLE I. Measured isotope shifts $\delta\nu^{192,A}$, change of the mean-square charge radius $\delta\langle r^2\rangle^{192,A}$, and quadrupole deformation parameter $\langle\beta_2^2\rangle^{1/2}$ evaluated from this work and the previous experiment [14] for Os isotopes.

A	$\delta\nu^{192,A}$ (GHz)	$\delta\langle r^2\rangle^{192,A}$ (fm^2)	$\langle\beta_2^2\rangle^{1/2}$
196	−3.36(99)[a]	0.177(55)	0.157(15)
194	−0.65(65)[a]	0.034(35)	0.147(10)
192	0.0 [b]	0.0	0.1667(12)[c]
190	1.22(30)[b]	−0.064(17)	0.1771(46)
189	2.02(28)[b]	−0.106(18)	0.1797(47)
188	3.30(27)[b]	−0.174(21)	0.1761(55)

[a]This work.
[b]From Ref. [14].
[c]From Ref. [51].

B. Nuclear structure of ^{194,196}Os

The evaluated quadrupole deformation parameter of $\langle\beta_2^2\rangle^{1/2} = 0.147(10)$ for ^{194}Os is consistent with the recent experiment [52], in which $|\beta_2| = 0.140(10)$ was evaluated from $B(E2: 0^+ \to 2^+)$. This result is also in agreement with the theoretical calculations, as shown in Table II. Nazarewicz *et al.* [53] predicted an oblate deformed ground state for ^{194}Os with $\beta_2 = -0.14$ from Hartree-Fock (HF) calculations. John *et al.* [54,55] predicted an oblate minimum in the potential energy surface for both ^{194}Os ($|\beta_2| \approx 0.14$) and ^{196}Os ($|\beta_2| \approx 0.11$) from symmetry-conserving configuration-mixing (SCCM) calculations. On the other hand, Wheldon *et al.* [8] proposed a prolate deformed ground state for ^{194}Os ($|\beta_2| = 0.16$) and an oblate shape for ^{196}Os ($|\beta_2| = 0.12$) from total Routhian surface (TRS) calculation, whereas the finite range droplet model (FRDM) [56] suggests a prolate deformation for both ^{194}Os ($\beta_2 = +0.153$) and ^{196}Os ($\beta_2 = +0.119$). The comparison between evaluated $\langle\beta_2^2\rangle^{1/2}$ and calculated results shows a good agreement for ^{194}Os. Furthermore, the systematic trend of $\delta\langle r^2\rangle$ and $\langle\beta_2^2\rangle^{1/2}$ suggests a shape transition at ^{194}Os, as discussed in the following paragraph.

Assuming an axial shape with a uniform nuclear charge distribution, the deformation parameter $\langle\beta_2^2\rangle^{1/2}$ of ^{196}Os was deduced for the first time from the IS measurement. The evaluated value of $\langle\beta_2^2\rangle^{1/2} = 0.157(15)$ is larger than the theoretical predictions. This discrepancy could be the consequence of the shape fluctuation between the axially deformed rotor and spherical vibrator. The fluctuation is suggested from the experimental energy ratio $E(4_1^+)/E(2_1^+) = 2.44$ of ^{196}Os [54], which is close to the γ-unstable limit of 2.5. Thus, it would

TABLE II. The quadrupole deformation parameter $\langle\beta_2^2\rangle^{1/2}$ values for ^{194,196}Os from this work and theoretical models [8,53,54,56].

A	This work	HF	SCCM	TRS	FRDM
194	0.147(10)	0.14	0.14	0.16	0.153
196	0.157(15)		0.11	0.12	0.119

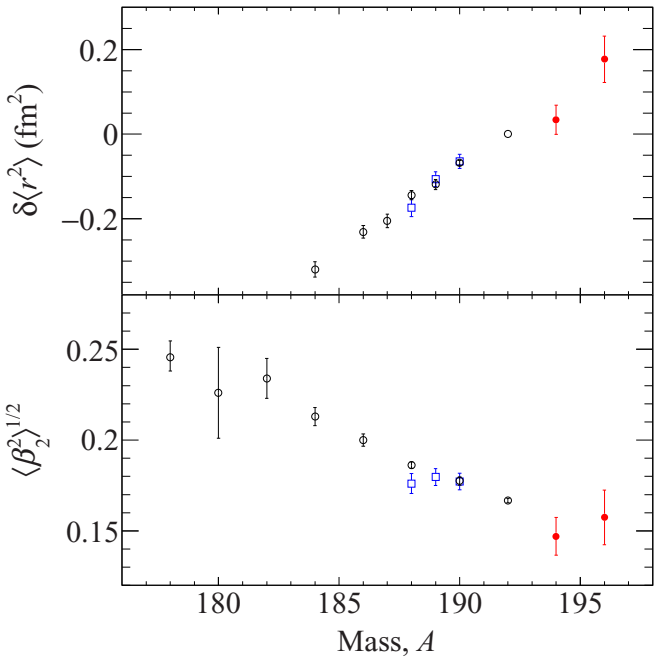

FIG. 5. Systematics of $\delta\langle r^2\rangle^{192,A}$ and $\langle\beta_2^2\rangle^{1/2}$ values for osmium isotopes. The black open, blue open, and red closed circles represent the values from Refs. [51,57,58], Ref. [14], and the present work, respectively.

be hard to discuss $\langle\beta_2^2\rangle^{1/2}$ based on the axially symmetric deformation.

Figure 5 shows the systematics of mean-square charge radius variation $\delta\langle r^2\rangle^{192,A}$ and quadrupole deformation parameter $\langle\beta_2^2\rangle^{1/2}$ as a function of mass number A for osmium isotopes. In the systematics, there is an increasing trend in $\delta\langle r^2\rangle^{192,A}$ and a decreasing trend in $\langle\beta_2^2\rangle^{1/2}$ as the $N = 126$ closed shell is approached. The systematics show an almost linear change in $\delta\langle r^2\rangle^{192,A}$ and $\langle\beta_2^2\rangle^{1/2}$ with increasing neutron numbers up to $A = 192$. However, a rapid change in both $\delta\langle r^2\rangle^{192,A}$ and $\langle\beta_2^2\rangle^{1/2}$ occurs at $A = 194$ compared to the trend in the lighter isotopes. This could indicate the shape transition from a prolate shape to a less deformed oblate configuration at $A = 194$, as expected by theoretical predictions [7,10].

This shape transition can be interpreted by the evolution of single-particle energies (SPEs), which is discussed in Ref. [3] for tungsten ($Z = 74$) isotopes by using Hartree-Fock-Bogoliubov (HFB) calculations. Here, we assumed that this interpretation is general in this region and can be applied to the osmium ($Z = 76$) isotopes. With increasing neutron number, the energy gaps between the Fermi level and $\pi(3s_{1/2})$, and $\nu(2f_{5/2})$ in the prolate side become smaller. On the other hand, the gap in the oblate side remains. Therefore, the shape transition from prolate to oblate occurs in this heavy region.

V. SUMMARY AND OUTLOOK

We performed in-gas-cell laser spectroscopy of neutron-rich nuclei ^{194}Os and ^{196}Os, which were produced by MNT reactions at KISS. The laser ionized Os isotopes were identified via conventional β-decay spectroscopy and newly applied time-of-flight mass spectrometry using MRTOF-MS. The resonant laser spectroscopy combined with the MRTOF-MS allowed us to identify ^{194,196}Os in a short measurement time with high mass resolving power of $R_m \approx 120\,000$. From the study of resonance spectra, the isotope shifts of two isotopes have been evaluated to be $\delta\nu^{192,194} = -0.65(65)$ GHz and $\delta\nu^{192,196} = -3.36(99)$ GHz for the transition $\lambda_1 = 247.7583$ nm. The corresponding $\delta\langle r^2\rangle^{192,A}$ and $\langle\beta_2^2\rangle^{1/2}$ for ^{194,196}Os were evaluated based on the pairing-plus-quadrupole model [28]. The calculated $\langle\beta_2^2\rangle^{1/2}$ of ^{194}Os is consistent with the recent experiment [52] and theoretical calculations. On the other hand, that of ^{196}Os shows a discrepancy from the theoretical predictions, which could be the consequence of its γ-unstable nature. In the systematics of $\delta\langle r^2\rangle^{192,A}$ and $\langle\beta_2^2\rangle^{1/2}$ for Os isotopes, a sudden change in the increasing or decreasing trend at $A = 194$ suggests a shape transition to a less deformed structure. To clarify this feature, more precise measurements using in-gas-jet laser spectroscopy [19,59] will be performed as part of a future plan. Moreover, with a sustained mass resolving power of 250 000, we will be able to fully resolve ^{196}Os from neighboring isobars and better resolve ^{194}Os.

ACKNOWLEDGMENTS

This experiment was performed at the RI Beam Factory operated by RIKEN Nishina Center and CNS, University of Tokyo. The authors acknowledge the RIKEN accelerator staff for their support. The authors wish to acknowledge Prof. I. Hamamoto (RIKEN, Japan) for her valuable comments in interpreting the nuclear structure of ^{196}Os isotope. This work was supported by Japan Society for the Promotion of Science KAKENHI Grants No. JP23244060, No. JP24740180, No. JP26247044, No. JP15H02096, No. JP17H01132, No. JP17H06090, and No. JP18H03711. This work was supported by the National Research Foundation of Korea Grants No. NRF-2016K1A3A7A09005575 and No. NRF-2019K2A9A2A10017576. This work was supported by the Rare Isotope Science Project of the Institute for Basic Science funded by Ministry of Science and ICT and National Research Foundation of Korea of Republic of Korea (2013M7A1A1075764).

[1] P. D. Stevenson, M. P. Brine, Z. Podolyak, P. H. Regan, P. M. Walker, and J. R. Stone, Phys. Rev. C **72**, 047303 (2005).
[2] P. Sarriguren, R. Rodríguez-Guzmán, and L. M. Robledo, Phys. Rev. C **77**, 064322 (2008).
[3] L. M. Robledo, R. Rodríguez-Guzmán, and P. Sarriguren, J. Phys. G **36**, 115104 (2009).
[4] R. Rodríguez-Guzmán, P. Sarriguren, L. M. Robledo, and J. E. García-Ramos, Phys. Rev. C **81**, 024310 (2010).

[5] P. Bond, R. Casten, D. Warner, and D. Horn, Phys. Lett. B **130**, 167 (1983).

[6] A. Ansari, Phys. Rev. C **33**, 321 (1986).

[7] K. Nomura, T. Otsuka, R. Rodríguez-Guzmán, L. M. Robledo, and P. Sarriguren, Phys. Rev. C **84**, 054316 (2011).

[8] C. Wheldon, J. Garcés Narro, C. J. Pearson, P. H. Regan, Z. Podolyák, D. D. Warner, P. Fallon, A. O. Macchiavelli, and M. Cromaz, Phys. Rev. C **63**, 011304(R) (2000).

[9] R. Casten, A. Namenson, W. Davidson, D. Warner, and H. Borner, Phys. Lett. B **76**, 280 (1978).

[10] K. Nomura, T. Otsuka, R. Rodríguez-Guzmán, L. M. Robledo, P. Sarriguren, P. H. Regan, P. D. Stevenson, and Z. Podolyák, Phys. Rev. C **83**, 054303 (2011).

[11] A. P. Hines and J. S. Ross, Phys. Rev. **126**, 2105 (1962).

[12] P. Aufmuth and E. Wöbker, Z. Phys. A: At. Nucl. **321**, 65 (1985).

[13] S. Kröger, G. Başar, A. Baier, and G. H. Guthöhrlein, Phys. Scr. **65**, 56 (2002).

[14] Y. Hirayama, M. Mukai, Y. Watanabe, M. Oyaizu, M. Ahmed, Y. Kakiguchi, S. Kimura, H. Miyatake, P. Schury, M. Wada, and S.-C. Jeong, J. Phys. B **50**, 215203 (2017).

[15] Y. Hirayama, M. Mukai, Y. X. Watanabe, M. Ahmed, S. C. Jeong, H. S. Jung, Y. Kakiguchi, S. Kanaya, S. Kimura, J. Y. Moon, T. Nakatsukasa, M. Oyaizu, J. H. Park, P. Schury, A. Taniguchi, M. Wada, K. Washiyama, H. Watanabe, and H. Miyatake, Phys. Rev. C **96**, 014307 (2017).

[16] T. E. Cocolios, A. N. Andreyev, B. Bastin, N. Bree, J. Büscher, J. Elseviers, J. Gentens, M. Huyse, Y. Kudryavtsev, D. Pauwels, T. Sonoda, P. Van den Bergh, and P. Van Duppen, Phys. Rev. Lett. **103**, 102501 (2009).

[17] C. Granados, P. Creemers, R. Ferrer, L. P. Gaffney, W. Gins, R. de Groote, M. Huyse, Y. Kudryavtsev, Y. Martínez, S. Raeder, S. Sels, C. Van Beveren, P. Van den Bergh, P. Van Duppen, K. Wrzosek-Lipska, A. Zadvornaya, A. E. Barzakh, B. Bastin, P. Delahaye, L. Hijazi *et al.*, Phys. Rev. C **96**, 054331 (2017).

[18] R. Ferrer, N. Bree, T. Cocolios, I. Darby, H. D. Witte, W. Dexters, J. Diriken, J. Elseviers, S. Franchoo, M. Huyse, N. Kesteloot, Y. Kudryavtsev, D. Pauwels, D. Radulov, T. Roger, H. Savajols, P. V. Duppen, and M. Venhart, Phys. Lett. B **728**, 191 (2014).

[19] R. Ferrer *et al.*, Nat. Commun. **8**, 14520 (2017).

[20] Y. Hirayama, Y. Watanabe, N. Imai, H. Ishiyama, S. Jeong, H. Miyatake, M. Oyaizu, S. Kimura, M. Mukai, Y. Kim, T. Sonoda, M. Wada, M. Huyse, Y. Kudryavtsev, and P. V. Duppen, Nucl. Instrum. Methods Phys. Res. Sect. B **353**, 4 (2015).

[21] Y. Hirayama, Y. Watanabe, N. Imai, H. Ishiyama, S. Jeong, H. Jung, H. Miyatake, M. Oyaizu, S. Kimura, M. Mukai, Y. Kim, T. Sonoda, M. Wada, M. Huyse, Y. Kudryavtsev, and P. V. Duppen, Nucl. Instrum. Methods Phys. Res. Sect. B **376**, 52 (2016).

[22] Y. Hirayama, Y. Watanabe, M. Mukai, M. Oyaizu, M. Ahmed, H. Ishiyama, S. Jeong, Y. Kakiguchi, S. Kimura, J. Moon, J. Park, P. Schury, M. Wada, and H. Miyatake, Nucl. Instrum. Methods Phys. Res. Sect. B **412**, 11 (2017).

[23] M. Mukai, Y. Hirayama, Y. Watanabe, P. Schury, H. Jung, M. Ahmed, H. Haba, H. Ishiyama, S. Jeong, Y. Kakiguchi, S. Kimura, J. Moon, M. Oyaizu, A. Ozawa, J. Park, H. Ueno, M. Wada, and H. Miyatake, Nucl. Instrum. Methods Phys. Res. Sect. A **884**, 1 (2018).

[24] J. Y. Moon, S. C. Jeong, M. Wada, P. Schury, Y. X. Watanabe, Y. Hirayama, Y. Ito, M. Rosenbusch, S. Kimura, S. Ishizawa, T. Niwase, H. Wollnik, and H. Miyatake, RIKEN Accel. Prog. Rep. **52**, 138 (2018).

[25] J. G. Cubiss, A. E. Barzakh, M. D. Seliverstov, A. N. Andreyev, B. Andel, S. Antalic, P. Ascher, D. Atanasov, D. Beck, J. Bieroń, K. Blaum, C. Borgmann, M. Breitenfeldt, L. Capponi, T. E. Cocolios, T. Day Goodacre, X. Derkx, H. De Witte, J. Elseviers *et al.*, Phys. Rev. C **97**, 054327 (2018).

[26] B. A. Marsh, T. Day Goodacre, S. Sels, Y. Tsunoda, B. Andel, A. N. Andreyev, N. A. Althubiti, D. Atanasov, A. E. Barzakh, J. Billowes, K. Blaum, T. E. Cocolios, J. G. Cubiss, J. Dobaczewski, G. J. Farooq-Smith, D. V. Fedorov, V. N. Fedosseev, K. T. Flanagan, L. P. Gaffney, L. Ghys *et al.*, Nat. Phys. **14**, 1163 (2018).

[27] J. G. Cubiss, A. E. Barzakh, A. N. Andreyev, M. A. Monthery, N. Althubiti, B. Andel, S. Antalic, D. Atanasov, K. Blaum, T. E. Cocolios, T. D. Goodacre, R. P. de Groote, A. de Roubin, G. J. Farooq-Smith, D. V. Fedorov, V. N. Fedosseev, R. Ferrer, D. A. Fink, L. P. Gaffney, L. Ghys *et al.*, Phys. Lett. B **786**, 355 (2018).

[28] B. S. Reehal and R. A. Sorensen, Nucl. Phys. A **161**, 385 (1971).

[29] Y. X. Watanabe, Y. H. Kim, S. C. Jeong, Y. Hirayama, N. Imai, H. Ishiyama, H. S. Jung, H. Miyatake, S. Choi, J. S. Song, E. Clement, G. de France, A. Navin, M. Rejmund, C. Schmitt, G. Pollarolo, L. Corradi, E. Fioretto, D. Montanari, M. Niikura, D. Suzuki, H. Nishibata, and J. Takatsu, Phys. Rev. Lett. **115**, 172503 (2015).

[30] R. P. de Groote, M. Verlinde, V. Sonnenschein, K. T. Flanagan, I. Moore, and G. Neyens, Phys. Rev. A **95**, 032502 (2017).

[31] T. Y. Hirsh, N. Paul, M. Burkey, A. Aprahamian, F. Buchinger, S. Caldwell, J. A. Clark, A. F. Levand, L. L. Ying, S. T. Marley, G. E. Morgan, A. Nystrom, R. Orford, A. P. Galván, J. Rohrer, G. Savard, K. S. Sharma, and K. Siegl, Nucl. Instrum. Methods Phys. Res. Sect. B **376**, 229 (2016).

[32] R. Wolf, D. Beck, K. Blaum, C. Böhm, C. Borgmann, M. Breitenfeldt, F. Herfurth, A. Herlert, M. Kowalska, S. Kreim, D. Lunney, S. Naimi, D. Neidherr, M. Rosenbusch, L. Schweikhard, J. Stanja, F. Wienholtz, and K. Zuber, Nucl. Instrum. Methods Phys. Res. Sect. A **686**, 82 (2012).

[33] C. Jesch, T. Dickel, W. R. Plaß, D. Short, S. Ayet San Andres, J. Dilling, H. Geissel, F. Greiner, J. Lang, K. G. Leach, W. Lippert, C. Scheidenberger, and M. I. Yavor, Hyperfine Interact. **235**, 97 (2015).

[34] F. Wienholtz, D. Beck, K. Blaum, C. Borgmann, M. Breitenfeldt, R. B. Cakirli, S. George, F. Herfurth, J. D. Holt, M. Kowalska, S. Kreim, D. Lunney, V. Manea, J. Menéndez, D. Neidherr, M. Rosenbusch, L. Schweikhard, A. Schwenk, J. Simonis, J. Stanja, R. N. Wolf, and K. Zuber, Nature (London) **498**, 346 (2013).

[35] P. Schury, M. Wada, Y. Ito, D. Kaji, F. Arai, M. MacCormick, I. Murray, H. Haba, S. Jeong, S. Kimura, H. Koura, H. Miyatake, K. Morimoto, K. Morita, A. Ozawa, M. Rosenbusch, M. Reponen, P.-A. Söderström, A. Takamine, T. Tanaka, and H. Wollnik, Phys. Rev. C **95**, 011305(R) (2017).

[36] W. Plaß, T. Dickel, S. Purushothaman, P. Dendooven, H. Geissel, J. Ebert, E. Haettner, C. Jesch, M. Ranjan, M. Reiter, H. Weick, F. Amjad, S. Ayet, M. Diwisch, A. Estrade, F. Farinon, F. Greiner, N. Kalantar-Nayestanaki, R. Knöbel *et al.*, Nucl. Instrum. Methods Phys. Res. Sect. B **317**, 457 (2013).

[37] Y. Ito, P. Schury, M. Wada, F. Arai, H. Haba, Y. Hirayama, S. Ishizawa, D. Kaji, S. Kimura, H. Koura, M. MacCormick, H.

Miyatake, J. Y. Moon, K. Morimoto, K. Morita, M. Mukai, I. Murray, T. Niwase, K. Okada, A. Ozawa *et al.*, Phys. Rev. Lett. **120**, 152501 (2018).
[38] M. Rosenbusch, M. Wada, P. Schury, Y. Ito, H. Ishiyama, S. Ishizawa, Y. Hirayama, S. Kimura, T. Kojima, H. Miyatake, J. Moon, T. Niwase, T. Sonoda, A. Takamine, Y. Watanabe, and H. Wollnik, Nucl. Instrum. Methods Phys. Res. Sect. B **463**, 184 (2020).
[39] P. Schury *et al.*, RIKEN Accel. Prog. Rep. (to be published).
[40] P. Schury, Y. Ito, M. Rosenbusch, H. Miyatake, M. Wada, and H. Wollnik, Int. J. Mass Spectrom. **433**, 40 (2018).
[41] P. E. Haustein, E. M. Franz, R. F. Petry, and J. C. Hill, Phys. Rev. C **16**, 1559 (1977).
[42] http://www.nndc.bnl.gov/.
[43] Y. Ito, P. Schury, M. Wada, S. Naimi, T. Sonoda, H. Mita, F. Arai, A. Takamine, K. Okada, A. Ozawa, and H. Wollnik, Phys. Rev. C **88**, 011306(R) (2013).
[44] M. Wang, G. Audi, F. G. Kondev, W. J. Huang, S. Naimi, and X. Xu, Chin. Phys. C **41**, 030003 (2017).
[45] F. James, *MINUIT, Function Minimization and Error Analysis Reference Manual, Version 94.1*, ROOT CERN Program Library entry D506 (CERN, Geneva, 1994).
[46] K. Heilig and A. Steudel, At. Data Nucl. Data Tables **14**, 613 (1974).
[47] E. C. Seltzer, Phys. Rev. **188**, 1916 (1969).
[48] D. Verney, L. Cabaret, J. E. Crawford, H. T. Duong, B. Fricke, J. Genevey, G. Huber, F. Ibrahim, M. Krieg, F. Le Blanc, J. K. P. Lee, G. Le Scornet, D. Lunney, J. Obert, J. Oms, J. Pinard, J. C. Puteaux, K. Rashid, B. Roussière, J. Sauvage, V. Sebastian, and the ISOLDE Collaboration, Eur. Phys. J. A **30**, 489 (2006).
[49] S. Ahmad, W. Klempt, R. Neugart, E. Otten, P.-G. Reinhard, G. Ulm, and K. Wendt, Nucl. Phys. A **483**, 244 (1988).
[50] W. D. Myers and K.-H. Schmidt, Nucl. Phys. A **410**, 61 (1983).
[51] S. Raman, C. Nestor, and P. Tikkanen, At. Data Nucl. Data Tables **78**, 1 (2001).
[52] T. Daniel, S. Kisyov, P. H. Regan, N. Marginean, Z. Podolyák, R. Marginean, K. Nomura, M. Rudigier, R. Mihai, V. Werner, R. J. Carroll, L. A. Gurgi, A. Oprea, T. Berry, A. Serban, C. R. Nita, C. Sotty, R. Suvaila, A. Turturica, C. Costache, L. Stan, A. Olacel, M. Boromiza, and S. Toma, Phys. Rev. C **95**, 024328 (2017).
[53] W. Nazarewicz, M. Riley, and J. Garrett, Nucl. Phys. A **512**, 61 (1990).
[54] P. R. John, V. Modamio, J. J. Valiente-Dobón, D. Mengoni, S. Lunardi, T. R. Rodríguez, D. Bazzacco, A. Gadea, C. Wheldon, T. Alexander, G. de Angelis, N. Ashwood, M. Barr, G. Benzoni, B. Birkenbach, P. G. Bizzeti, A. M. Bizzeti-Sona, S. Bottoni, M. Bowry, A. Bracco *et al.*, Phys. Rev. C **90**, 021301 (2014).
[55] P. R. John, Ph.D. thesis, University of Padua, 2015.
[56] P. Möller, A. Sierk, T. Ichikawa, and H. Sagawa, At. Data Nucl. Data Tables **109–110**, 1 (2016).
[57] I. Angeli and K. Marinova, At. Data Nucl. Data Tables **99**, 69 (2013).
[58] B. Pritychenko, M. Birch, B. Singh, and M. Horoi, At. Data Nucl. Data Tables **107**, 1 (2016).
[59] Y. Kudryavtsev, R. Ferrer, M. Huyse, P. V. den Bergh, and P. V. Duppen, Nucl. Instrum. Methods Phys. Res. Sect. B **297**, 7 (2013).